Available online at www.sciencedirect.com

ScienceDirect

journal homepage: www.elsevier.com/locate/he

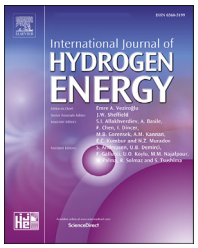

Investigation of photocatalytic, electrochemical, optical and magnetic behaviors of rare-earth double perovskites using combustion synthesized Gd_2NiMnO_6 nanostructures in the presence of different saccharides

Reza Mohassel [a], *Azam Sobhani* [b,**], *Masoud Salavati-Niasari* [a,*]

[a] *Institute of Nano Science and Nano Technology, University of Kashan, Kashan, P. O. Box. 87317–51167, Islamic Republic of Iran*

[b] *Department of Chemistry, Kosar University of Bojnord, Bojnord, Islamic Republic of Iran*

ARTICLE INFO

Article history:
Received 15 August 2018
Received in revised form
11 October 2018
Accepted 5 November 2018
Available online 28 November 2018

Keywords:
Gd_2NiMnO_6
Nanostructures
Combustion
Photocatalysis
Antiferromagnetism
Direct band gap

ABSTRACT

This paper reports combustion synthesis of Gd_2NiMnO_6 nanostructures (GNMO NSs), for the first time, through reaction between metal nitrates in the presence of different saccharides, as capping and reducing agents. Analysis of XRD, FT-IR, EDS, along with TEM and SEM images and also VSM and DRS spectra were applied to study the NSs. The VSM showed an antiferromagnetic behavior. The DRS spectroscopy ascertained semiconducting behavior of GNMO NSs with $E_g = 3.05$ eV for optimum sample prepared in the presence of glucose at 1000 °C. The CV was used to investigation of electrochemical property of the NSs. For the first time, the photocatalytic behavior of the GNMO NSs was evaluated, using the degradation of organic dyes under UV irradiation. The photodegradation of EDT was almost similar to that of ES, except for initial times of the irradiation. The degradation percentage of EBT and ES in the presence of GNMO NSs was large, whereas that of MV was little in the time range.

Introductions

Rare-earth double perovskites ($Ln_2BB'O_6$, Ln = rare earth) are an important class of materials, characterized by subtle structural distortions from the cubic aristotype structure [1]. Displacements of the Ln and B cations within the cage and also concerted rotations of the BO_6 octahedra cause these distortions, that are dependent on temperature and pressure [1]. The distortions give rise to dramatic changes in dielectric property, electrical resistivity, band gap etc. In $Ln_2BB'O_6$, the B site cations are often assumed to be disordered, and the average unit cell size and symmetry of the aristotype are unaffected [2]. In these perovskites, ordering among the B site cations causes lowering of the perovskite symmetry, in addition to distortion of the metal sites, and tilting of the octahedra [2]. The B cation has partially filled e_g orbitals whereas B′ has empty e_g orbitals orvice-versa [3]. The Ln and B site

* *Corresponding author.*
** *Corresponding author.*
E-mail addresses: sobhani@kub.ac.ir (A. Sobhani), salavati@kashanu.ac.ir (M. Salavati-Niasari).
https://doi.org/10.1016/j.ijhydene.2018.11.034
0360-3199/

substitutions in these perovskites can be adjusted to provide materials with highly dependent magnetic and electronic behaviors [2]. The Gd_2NiMnO_6 studied here constitute one such series of compounds. The Gd and Gd based alloys have been received large attention because large magnetic moment of Gd [4,5].

Recently, Ln_2NiMnO_6 ceramics have attracted extensive research attention because of their rich physics and prospects for technological applications, such as electronic, magnetic [2], magnetoelectric [6–8], magnetodielectric [9], magnetocaloric [10], ferromagnetic and ferroelectric characteristics [11–13] and also colossal magnetoresistance, magnetocapacitance, room temperature ferromagnetism etc [14]. In Ln_2CoMnO_6 coexistence of electrocaloric and magnetocaloric effects with multicaloric coupling has excited the role of double perovskites in solid state refrigeration applications [15]. Balli et al. investigated these applications in La_2NiMnO_6 and La_2CoMnO_6 compounds [16,17]. Goodenough showed a systematic decrease in the magnetic ordering Curie temperature in Ln_2NiMnO_6 ceramics, as a function of decreasing lanthanide ionic radius [18]. Bull et al. investigated the $Ln_2BB'O_6$ perovskites by Raman scattering spectroscopy [2]. They showed that there is no significant change in the octahedral distortion in the Ln_2CoMnO_6 and Ln_2NiMnO_6, upon decreasing the lanthanide ionic radius. By decreasing orbital overlap within the BO_6 sublattice, in the $Ln_2BB'O_6$, magnetic and electrical properties of these materials can be changed. The variation in B–O–B′ angles associated with the tilting is used to understand these properties [2]. Bull demonstrated that the transition metal oxidation states in Ln_2NiMnO_6 ceramics are non-integral and showed systematic changes in the band gap with lanthanide cation radius [2]. Choudhury et al. showed the magnetodielectric effect in La_2NiMnO_6 originates from asymmetric hopping between neighbouring magnetic ions with relative spin orientations [9]. They observed this effect strongly at room temperature, even above the magnetic transition temperature [9]. Oh et al. investigated magnetodielectric effect in Gd_2NiMnO_6 [19]. Mohapatra showed that Gd_2NiMnO_6 exhibits a magnetic transition (TN) at ~125 K [20]. Also, he investigated structural, low temperature dielectric and magnetic properties of this ceramic [14].

In the present work, we have chosen Gd and prepared the GNMO compound. The strong exchange interactions between (Ni/Mn)-3d and Gd-4f magnetic sub-lattices and the field sensitive magnetic configurations of GNMO are expected to trigger interesting magnetic phenomena. We have synthesized GNMO ceramic as there is fairly sparse study as compared to that of La_2NiMnO_6. Different methods have used to synthesize various functional inorganic oxide nanostructures and its property-applications [21–28]. Among these methods, the combustion synthesis generates reproducibly high purity products in short times. The obtained products by this method have controlled shapes and sizes. To our knowledge, it is the first time that combustion method and also saccharides are used for the synthesis of the GNMO. This work is first attempt on the study of effects of mono, di and polysaccharides and also temperature on the morphology, particle size and properties of the GNMO NSs. There is no previous report concerning the investigation of the photocatalytic activity of GNMO, thus, the present investigation focuses on the study of this property. Also it is the first time that electrochemical behavior and also band gap of GNMO are investigated.

Experimental

Materials and experiments

All reagents were of analytical grade and were used without further treatment. FE-SEM and TEM images were obtained by TESCAN Mira3 FE-SEM and Philips EM208 transmission electron (200 Kv voltage) microscopes, respectively. A diffractometer of Philips company with X'PertPro monochromatized Cu Kα radiation was used to collect XRD patterns ($\lambda = 1.54$ Å). A XL30 Philips microscope was used for EDS analysis. Fourier transform infrared spectrum (FT-IR) of the GNMO NSs was record by a Nicolet Magna- 550 spectrophotometer in KBr pellets. The magnetic properties of the samples were detected at room temperature using a vibrating sample magnetometer (VSM, Meghnatis Kavir Kashan Co., Kashan, Iran). Diffuse reflectance spectrum (DRS) of the GNMO NSs was taken by a V-670 UV–Vis–NIR spectrophotometer (Jasco). Voltammetric study was carried out by Sama 500 potentiostat (Isfahan in Iran).

Synthesis of Gd_2NiMnO_6 nanostructures

The GNMO NSs were prepared by combustion method using high purity precursor materials, $Gd(NO_3)_3$, $Ni(NO_3)_2$, $Mn(NO_3)_2.6H_2O$. An aqueous solution of carbohydrate was prepared (20 ml). In this synthesis, five different carbohydrates including maltose (2.95 g), lactose (2.95 g), starch (1.4 g), fructose (1.55 g) and glucose (1.55 g) were used as capping and reducing agents. Three aqueous solutions of metal nitrates were prepared with stoichiometric ratio 2:1:1 of Gd:Ni:Mn. 0.3 g $Gd(NO_3)_3$, 0.096 g $Ni(NO_3)_2$ and 0.083 g $Mn(NO_3)_2.6H_2O$ were solved in 10 ml water, separately. The Gd, Ni and Mn solutions were added to the aqueous solution of the carbohydrate, respectively. After stirring the solution for 30 min at 60 °C and then at 100 °C, a highly viscous gel formed. The gel was dried in an oven at 75 °C for 24 h. The final residue was calcined at 800 °C for 5 h. The reaction conditions for the synthesis of GNMO NSs have been listed in Table 1. Scheme 1 shows a diagram illustrating the formation of GNMO NSs.

Photocatalytic tests

The photocatalytic activity of GNMO NSs was checked by the decomposition of three organic dyes, methyl violet (MV), erythrosine (ES) and eriochrome Black T (EBT), under UV illumination with a 125 W mercury lamp. The photocatalytic reactions were performed in a quartz reactor at room temperature. Utilizing a thermostatic water bath, the temperature of the mixture was kept constant. The catalyst powder (50 mg) was suspended in 50 mL of dye solutions (5 ppm). The mixture was magnetically stirred and bubbled with air (10 mL/min) during the photocatalytic tests. Prior to UV irradiation, the catalyst suspension was dispersed by a magnetic stirrer for 30 min in the dark, to achieve adsorption equilibrium. During

Table 1 – The reaction conditions of GNMO NSs synthesized in this work.

Sample	Effect	Capping/ reducing agent	Gd:Capping agent	Calcination Temperature(C)	Time (h)	Morphology	Size
M800		Maltose (2.95 g)	1:13	800	5	Aggregated semi-spherical structures	–
L800	Capping/reducing	Lactose (2.95 g)	1:13	800	5	Aggregated semi-spherical structures	–
S800	agents	Starch (1.4 g)	1:13	800	5	Coalesced particles and bulk structures	–
F800		Fructose (1.55 g)	1:13	800	5	Shapeless nanostructures	–
G800		Glucose (1.55 g)	1:13	800	5	Semi-spherical nanostructures	70–150 nm
G900	Temperature	Glucose (1.55 g)	1:13	900	5	Semi-spherical nanostructures	50–200 nm
G1000		Glucose (1.55 g)	1:13	1000	5	Semi-spherical nanostructures	30–60 nm

irradiation, the catalyst was kept in suspension state by a magnetic stirrer. The quartz reactor and light source were placed inside a black box equipped with a fan to prevent UV leakage. Percentage of degradation (% D) is calculated according to % D = $\{(A_0 - A)/A_0\} \times 100$ equation [29], where A_0 and A are the absorbance of the liquid solutions at the beginning time (t_0) of photocatalytic treatment and at time t, respectively.

Results and discussion

It is suggested that the following reactions occur in this work. The $Gd(NO_3)_3$, $Mn(NO_3)_2.6H_2O$ and $Ni(NO_3)_2$ salts are reduced by glucose (Eqs. (1)–(3). After stirring the solution and formation of the gel and then calcination at 800 °C, metal oxides are formed (Eqs. (4)–(6)). Reaction of the Gd_2O_3 with MnO_2 and NiO is caused to formation of Gd_2NiMnO_6 (Eq. (7)):

$$Gd(NO_3)_3 + \text{Glucose} \rightarrow Gd(OH)_3 + \text{other products} \quad (1)$$

$$Mn(NO_3)_2.6H_2O + \text{Glucose} \rightarrow Mn(OH)_2 + \text{other products} \quad (2)$$

$$Ni(NO_3)_2 + \text{Glucose} \rightarrow Ni(OH)_2 + \text{other products} \quad (3)$$

$$2Gd(OH)_3 \rightarrow Gd_2O_3 + 3H_2O \quad (4)$$

$$2Mn(OH)_2 + O_2 \rightarrow 2MnO_2 + 2H_2O \quad (5)$$

$$Ni(OH)_2 \rightarrow NiO + H_2O \quad (6)$$

$$Gd2O_3 + MnO_2 + NiO \rightarrow Gd_2NiMnO_6 \quad (7)$$

The structure and morphology of the as-prepared GNMO ceramics were investigated by SEM and TEM images. Figs. 1 and 2 show the SEM images of samples prepared in the presence of different capping agents. Five types of saccharides, including two monohydrates (glucose, fructose), two dehydrates (maltose, lactose) and one polyhydrate (starch) were used as capping and reducing agents. The SEM images in Fig. 1a and b shows that aggregated semi-spherical structures are obtained, when maltose is used as capping agent. When

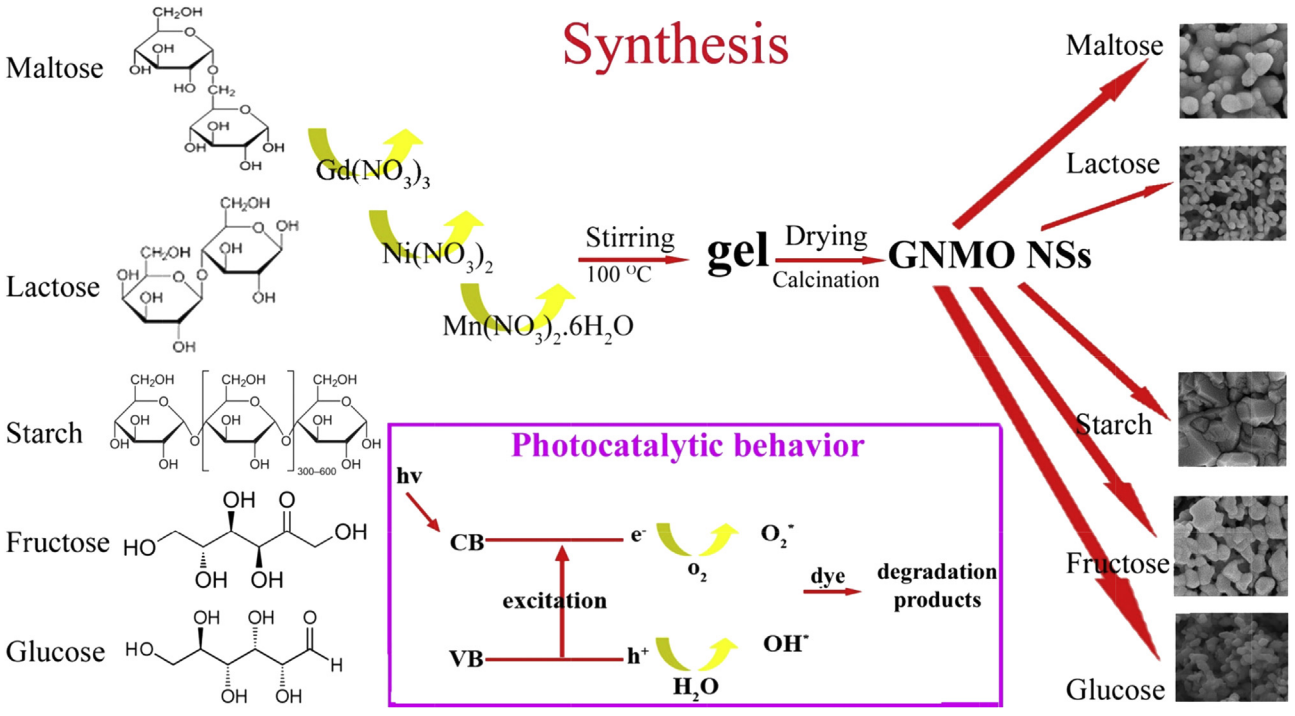

Scheme 1 – Diagram illustrating the formation of GNMO NSs.

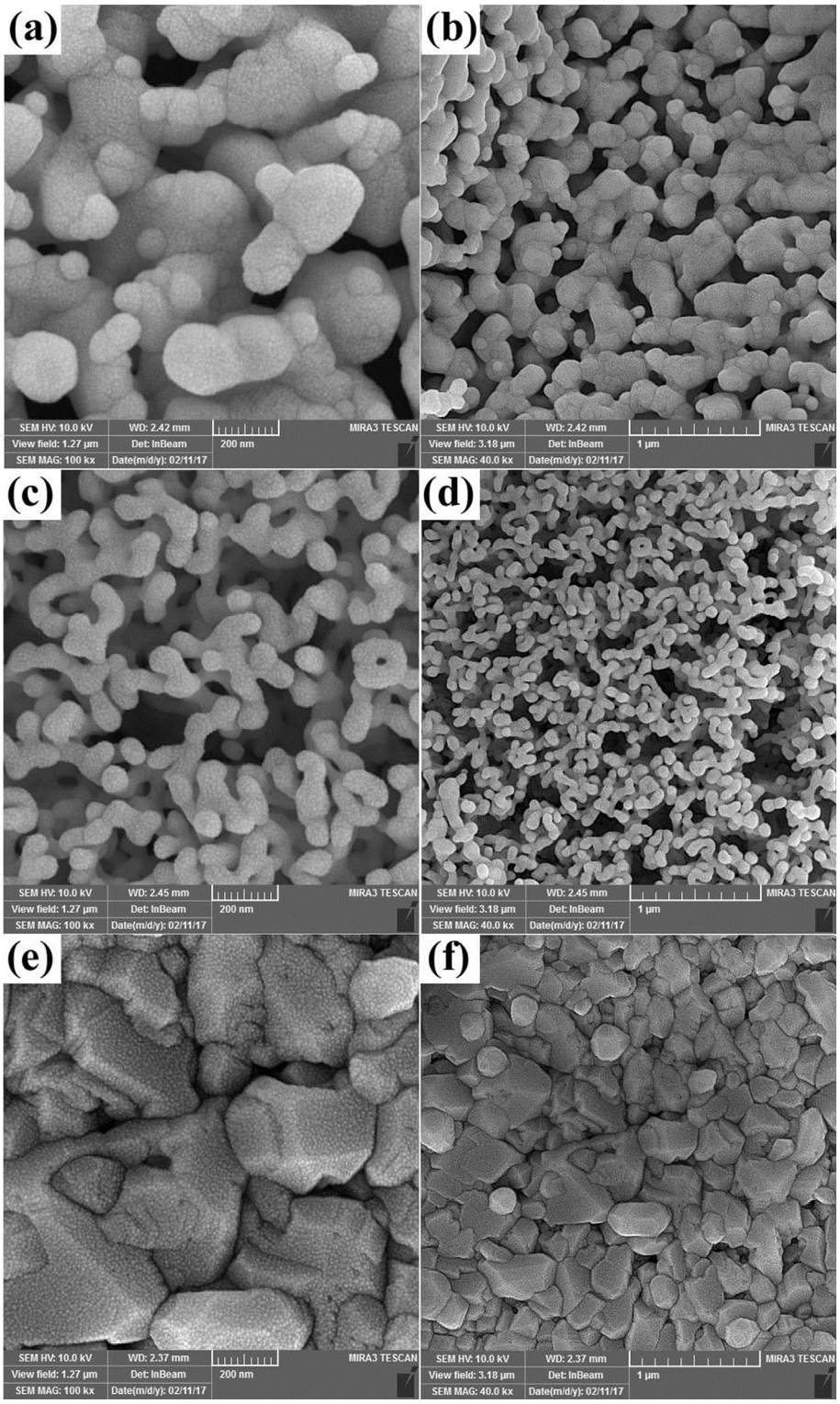

Fig. 1 – SEM images of the GNMO NSs at 800 °C for 5 h, in the presence of different stabilizing agents: (a, b) maltose (M800), (c, d) lactose (L800), (e, f) starch (S800).

maltose is substituted with lactose and other reaction parameters remained unchanged, aggregated semi-spherical nanostructures with smaller sizes are formed, as shown in Fig. 1c and d. Coalesced particles and bulk structures are formed in the presence of starch (Fig. 1e and f).

Fig. 2 shows SEM images of GNMO ceramics prepared in the presence of monohydrates. The products obtained in the presence of monohydrates, in our experimental conditions, are agglomerated nanoparticles. GNMO nanoparticles obtained in the presence of fructose and glucose have a particle

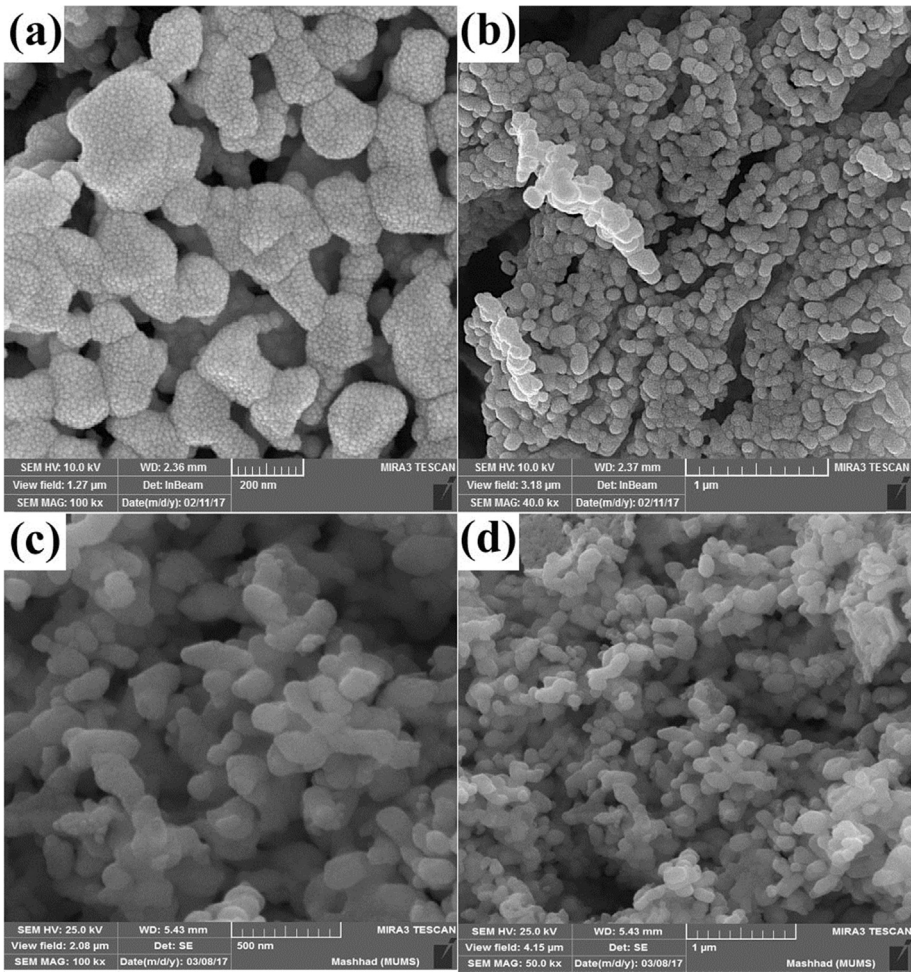

Fig. 2 – SEM images of the GNMO NSs at 800 °C for 5 h, in the presence of different stabilizing agents: (a, b) fructose (F800), (c, d) glucose (G800).

size lower than 10 nm and 50 nm, respectively (Fig. 2a–d, respectively). Shapeless and semi-spherical nanostructures are formed from agglomeration of these nanoparticles, in F800 and G800 obtained in the presence of fructose and glucose, respectively.

Considering different saccharides employed to prepare the GNMO ceramics, from Figs. 1 and 2, it is obvious that using monohydrates as capping and reducing agents decreases the particle size of the products and is preferred for the GNMO ceramic synthesis. The structures of the different saccharides used in this work, have been shown in Scheme 1. The saccharides contain –OH, –O– and =O functional groups. Due to open chain structures in monosaccharides, these functional groups are more accessible than those in di/polysaccharides. The more accessible functional groups in monosaccharides protect nanoparticles from further aggregation and limit the size of them, thus play an important role in the formation of the nanoparticles and semi-spherical nanostructures. Thus our group was continued synthesis of GNMO ceramics in the presence of the glucose, at different temperatures from 800 to 1000 °C. Fig. 3 shows effect of reaction temperature on the morphology and shape of the as-synthesized products in the presence of glucose. This figure also shows formation of the agglomerated semi-spherical nanostructures from agglomeration of the nanoparticles, in the presence of glucose at 900 and 1000 °C. The obtained semi-spherical nanostructures at 800 °C (G800, Fig. 2c and d) and 900 °C (G900, Fig. 3a and b) have the diameters ranging from 70 to 150 nm and 50–200 nm, respectively. While Fig. 3c and d shows that semi-spherical nanostructures obtained in the presence of the glucose at 1000 °C (G1000), have a nearly uniform distribution with an average diameter about 100 nm. Thus, in our experimental conditions, G1000 was selected an optimum product. With increasing of the temperature, morphology of the samples remains nearly constant and only size and agglomeration of the nanoparticles change. With respect to above mentioned, reaction temperature is one parameter to controlling the particle size of the products. Many fundamental properties of the materials are expressed as a function of the shape and size, thus control of growth and nucleation is becoming critical [30–35].

Fig. 4 presents TEM images of sample prepared in the presence of the glucose at 1000 °C (G1000). The images show formation of semi-spherical nanostructures with diameters 30–60 nm. The TEM results are in good agreement with the SEM results.

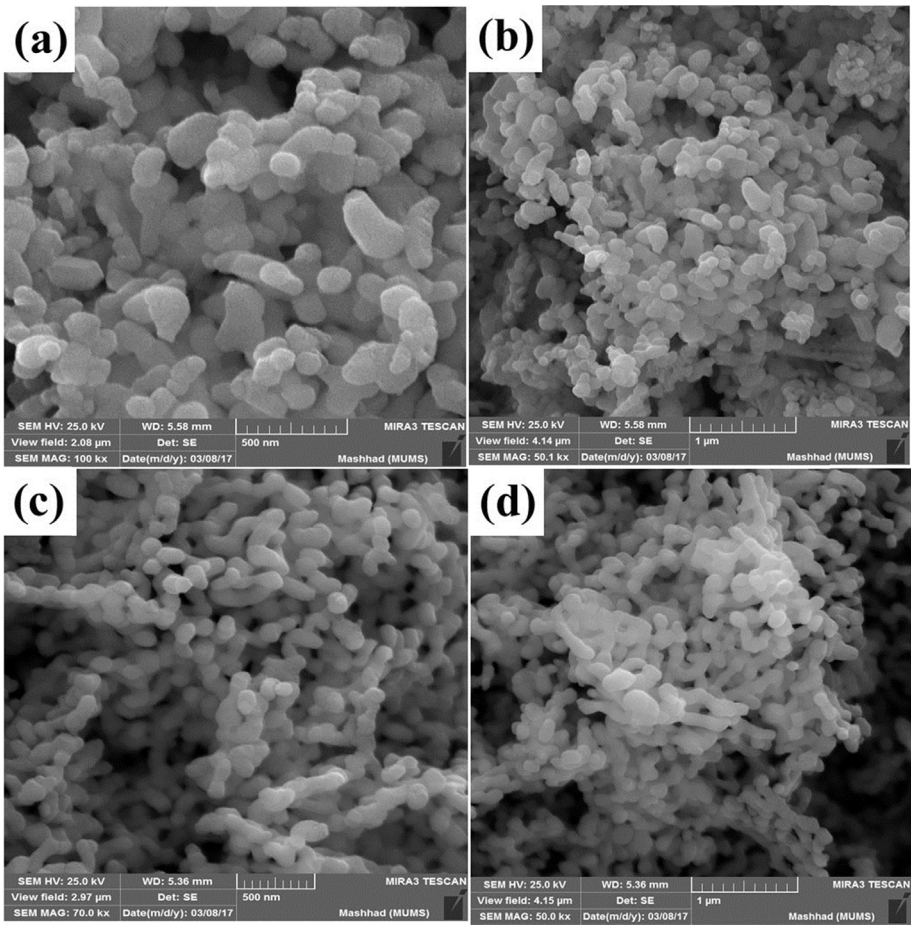

Fig. 3 – SEM images of the GNMO NSs in the presence of glucose at different temperatures: (a, b) 900 °C (G900), (c, d) 1000 °C (G1000).

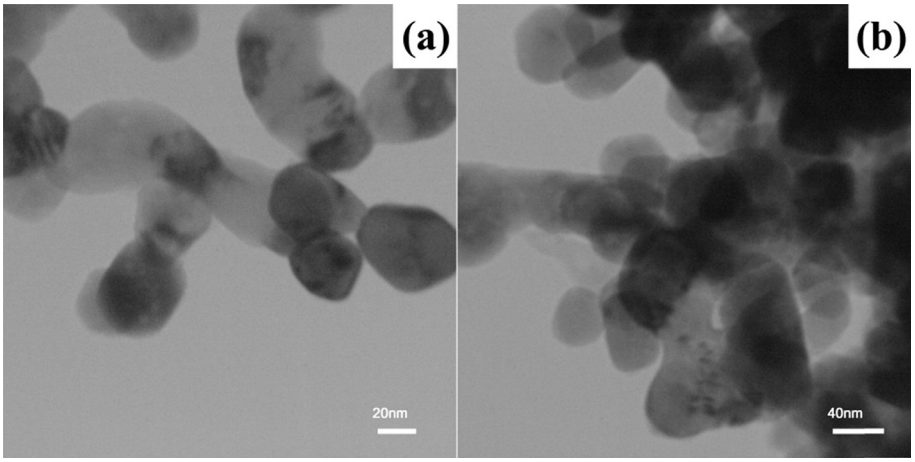

Fig. 4 – TEM images of the as-prepared GNMO NSs (G1000).

The crystal structure and composition of the as-prepared products are determined by XRD. Fig. 5a and b depicts XRD patterns of M800 and G1000 prepared in the presence of maltose and glucose, respectively. The M800 and G1000 are well crystallized due to sharp diffraction peaks in XRD patterns in Fig. 5a and b. As shown in Fig. 5a, in the presence of the maltose (M800), a mixture of Gd_2O_3 (JCPDS card No. 11-0608) and $GdNiO_3$ (JCPDS card No. 51-0392) are formed. The peaks indexed with red star in this figure, indicate Gd_2O_3 and other peaks show $GdNiO_3$. The product obtained in the presence of the glucose at 1000 °C (G1000) is Gd_2NiMnO_6 with orthorhombic crystal system and space group Pbnm. All diffraction peaks in the XRD pattern in Fig. 5b can be attributed to the Gd_2NiMnO_6. The functional groups are understood

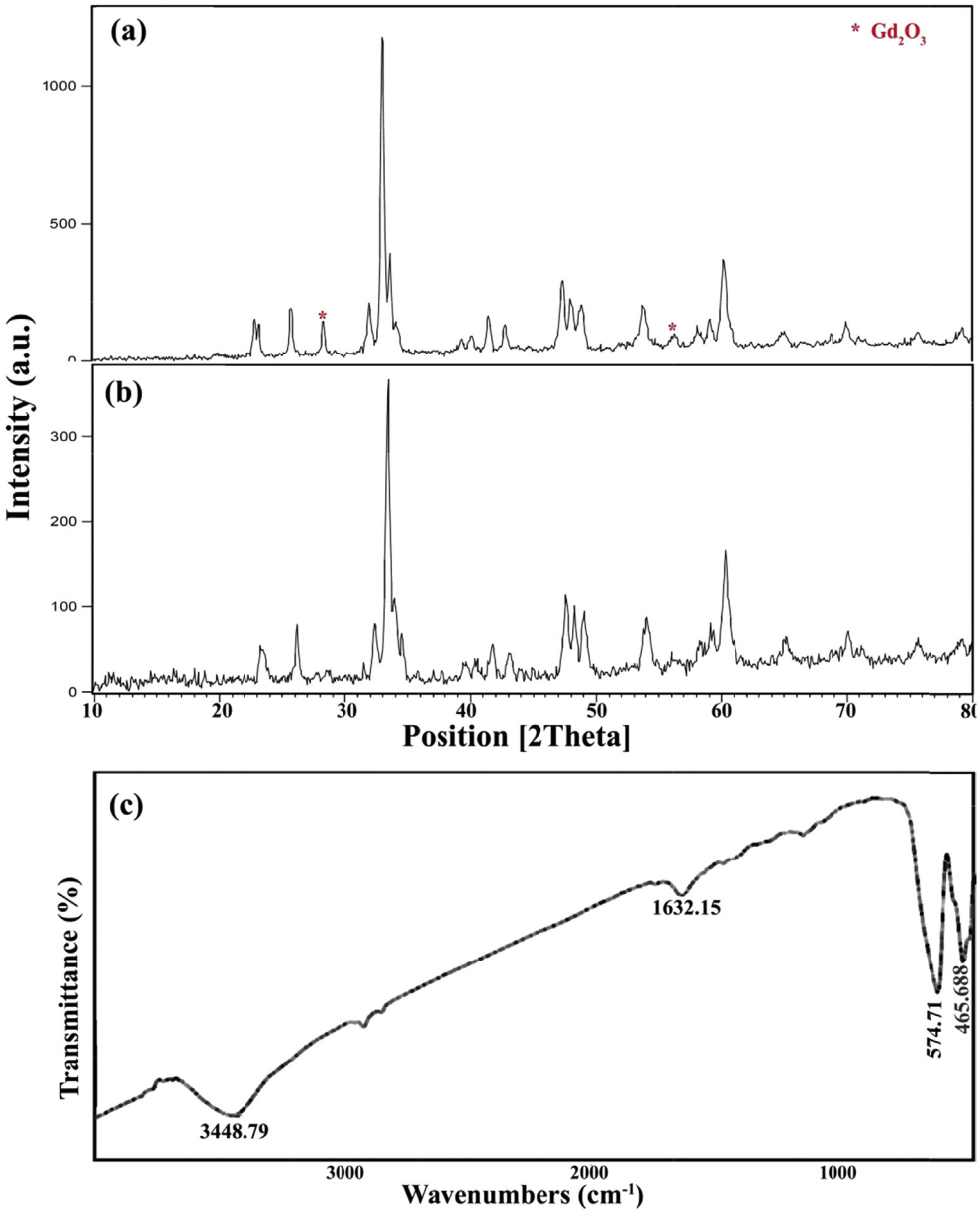

Fig. 5 – (a) XRD patterns of the GNMO NSs (a) M800, (b) G1000 and (c) FT-IR spectrum of G1000.

by FT-IR spectroscopy. FT-IR spectrum of G1000 is shown in Fig. 5c. We can see metal–oxygen stretching modes at ca. 580 and 433 cm^{-1} in semi-spherical nanostructures prepared in the presence of glucose at 1000 °C.

EDS analysis is also used for the evaluation of the composition of the GNMO NSs. Fig. 6a and b shows the EDS spectra of the M800 and G800 prepared in the presence of maltose and glucose, respectively. The figure indicates that the elements in both samples are Gd, Ni, Mn and O, and confirms formation of pure Gd_2NiMnO_6 and also XRD results. The EDS results have been summarized in Table 2.

Many molecules absorb UV or visible light. Different molecules absorb radiation of different wavelengths. When a molecule or atom absorbs energy, electrons are promoted from their ground state to an excited state. In a molecule, the atoms can rotate and vibrate with respect to each other. These vibrations and rotations also have discrete energy levels, which can be considered as being packed on top of each electronic level.

The absorption spectrum as a function of wavelength (in nm) for GNMO NSs is depicted in Fig. 7a. The figure shows the peaks in ranging 200–400 nm for G1000 prepared in the presence of glucose at 1000 °C. The absorption of UV or visible radiation corresponds to the excitation of outer electrons. There are three types of electronic transitions that involve different electrons, including p, s and n electrons, charge-transfer electrons, d and f electrons. The absorptions in Fig. 7a relate to the charge transfer (from 2p orbital of O to 3d orbital of transition metal) and d-d transitions (of the Jahn-Teller splitting) [36]. DRS spectroscopy ascertains

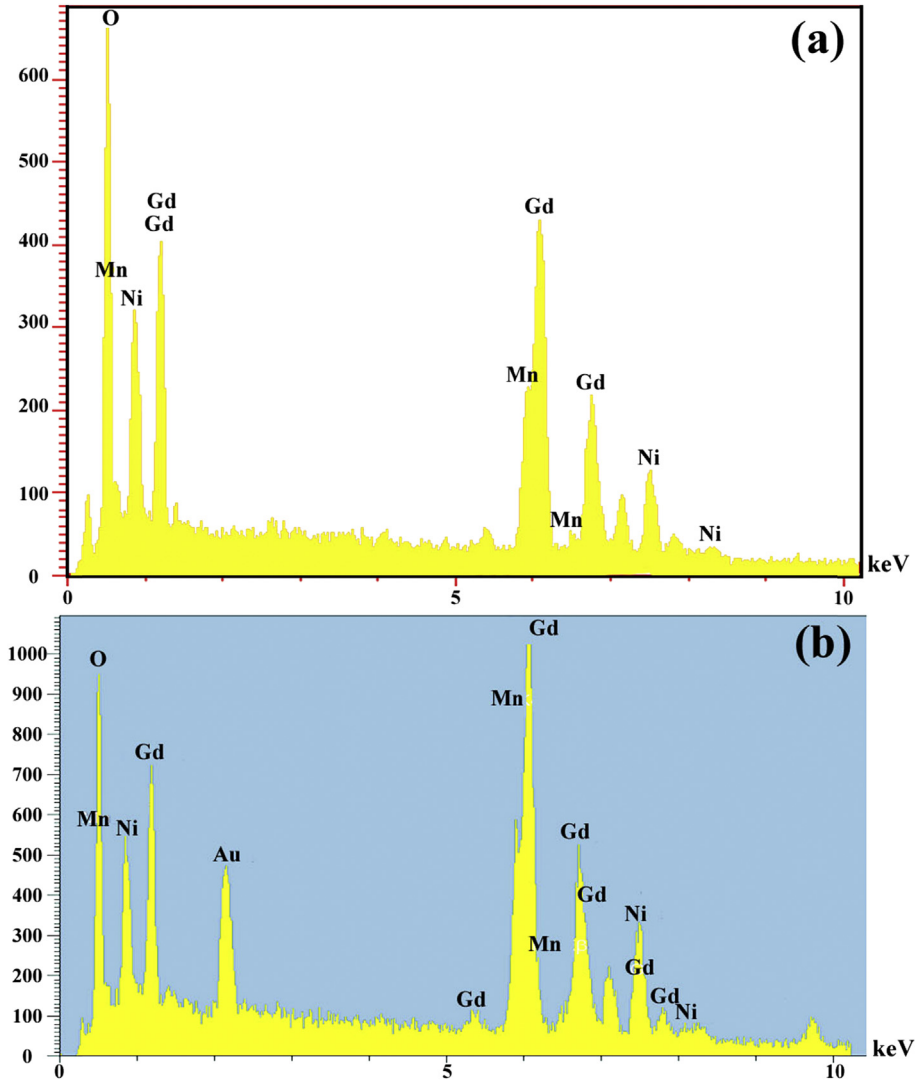

Fig. 6 – EDS patterns of the GNMO NSs: (a) M800, (b) G800.

semiconducting behavior of GNMO NSs prepared in this work. By using $\alpha h\upsilon = k(h\upsilon - E_g)^{n/2}$ equation, we can have an estimate of the optical band gap [37]. In this equation $h\upsilon$ = energy (in eV), E_g = gap energy, α = absorption coefficient, k and h = constants. Inset in Fig. 7 (Fig. 7b) shows curve of $(\alpha h\upsilon)^2$ against $h\upsilon$ for the GNMO NSs (G1000), also shows a direct transition for the NSs. The E_g of the GNMO NSs is determined by extrapolation of the linear portion of this curve to a point $(\alpha h\upsilon)^2 = 0$. The E_g value for G1000 is calculated to be 3.05 eV, which is larger than that in the GNMO prepared by the other routes. The blue shift of the E_g in the GNMO NSs prepared in this work improves their photo-absorption and photocatalytic performance and enables us to utilize them as photocatalysis.

Table 2 – Weight % and atomic % of elements in M800 and G800 (obtained from EDS results).

Elements	M800		G800	
	W%	A%	W%	A%
O	13.57	54.69	16.59	60.44
Mn	5.17	6.07	6.04	6.41
Ni	8.61	9.45	7.18	7.13
Gd	72.65	29.78	70.18	26.02
Total	100.00	100.00	100.00	100.00

Perovskites and double perovskites show different magnetic structures, including ferromagnetic, ferrimagnetic or antiferromagnetic [14]. Ln_2NiMnO_6 has been known as a ferromagnetic material [38,39]. Goodenough [40] and Blasse [41] suggested that the origin of ferromagnetism in this material is super-exchange interactions between Ni^{3+}–O–Mn^{3+} and Ni^{2+}–O–Mn^{4+}, respectively. Fig. 8 shows M–H hysteresis at 300 K for G1000. The GNMO NSs exhibit a linear variation of magnetization from low to high fields. According to this figure, G1000 has an antiferromagnetic (AFM) behavior (↓↓↑↑). The AFM ordering can be attributed to the presence of intrinsic anti-site disorder leading to distorting effect on the lattice. It

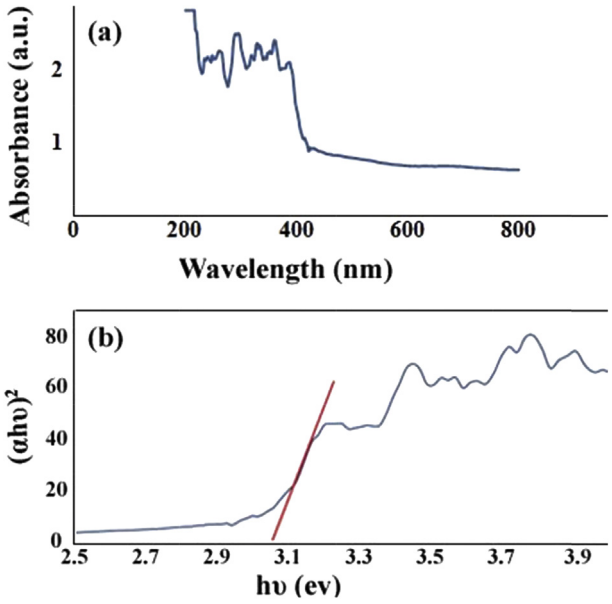

Fig. 7 – (a) DRS spectrum and (b) curve of $(\alpha h\upsilon)^2$ against hυ for the GNMO NSs (G1000).

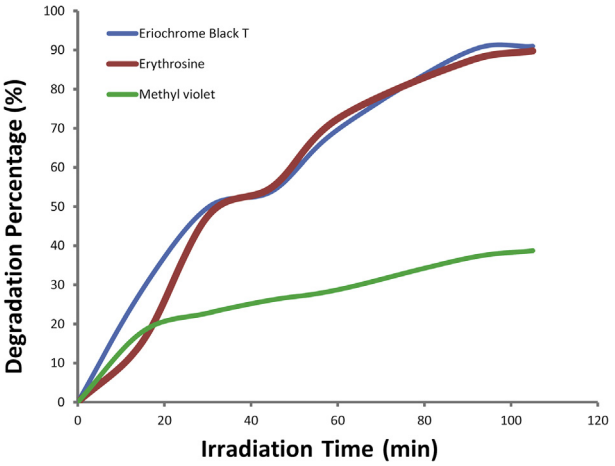

Fig. 9 – Photocatalytic activity of the GNMO NSs for degradation of different dyes.

also leading to Ni^{2+}–O^{2-}–Ni^{2+} and Mn^{4+}–O^{2-}–Mn^{4+} interactions, causing AFM ordering, in turn, leading to magnetic frustration [14]. This behavior is also due to polarization of Mn/Ni magnetic sublattices to the Gd moments.

Fig. 9 shows degradation percentage of EBT, ES and MV in the presence of the GNMO NSs as photocatalyst, under UV light. The photocatalysts are needed for effective degradation of the dyes [42–44]. The goal of choice of EBT, ES and MV in this work, is comparing the photocatalytic activity of cationic and anionic dyes. Boat EBT and ES are anionic dyes and Fig. 9 shows that their degradations are almost similar. This Figure shows photocatalytic behavior of anionic contaminants is better than cationic contaminant (MV). About %90 degradation of EBT and ES, in the presence of GNMO NSs, take places after 100 min under UV light, whereas about %35 MV is eliminated after 100 min irradiation. The weaker photocatalytic activity of MV compared to EBT and ES can be due to positive charge of MV and also absence of O groups in this dye. Presence of the O groups in EBT (as $-SO_3^-$, –OH) and also in ES (as $-O^-$, $-O^-$, =O, $-COO^-$) increases adsorption of the dye on the photocatalyst; and thus increases photocatalytic activity. The suggested mechanism of the photocatalytic degradation of the dyes can be assumed as:

$$GNMO \rightarrow GNMO\ (e^{-}_{CB} + h^{+}_{VB})$$

$$GNMO\ (h^{+}_{VB}) + H_2O \rightarrow GNMO + H^+ + OH^{\cdot}$$

$$GNMO\ (e^{-}_{CB}) + O_2 \rightarrow GNMO + O_2^{\cdot-}$$

$$O_2^{\cdot-} + H^+ \rightarrow HO_2^{\cdot}$$

$$Dye + OH^{\cdot} \rightarrow degradation$$

$$Dye + h^{+}_{VB} \rightarrow oxidation$$

$$Dye + e^{-}_{CB} \rightarrow reduction$$

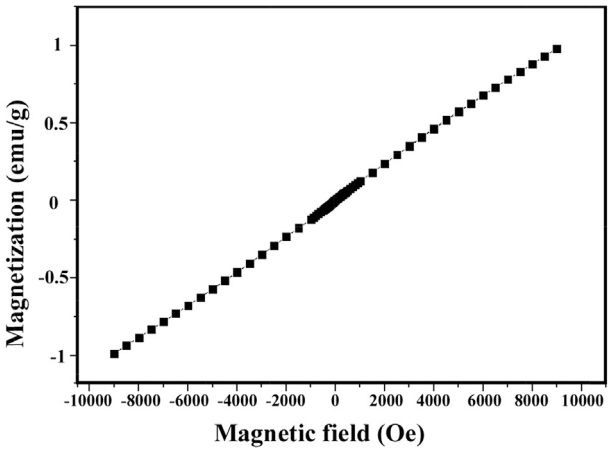

Fig. 8 – M–H hysteresis at 300 K for G1000.

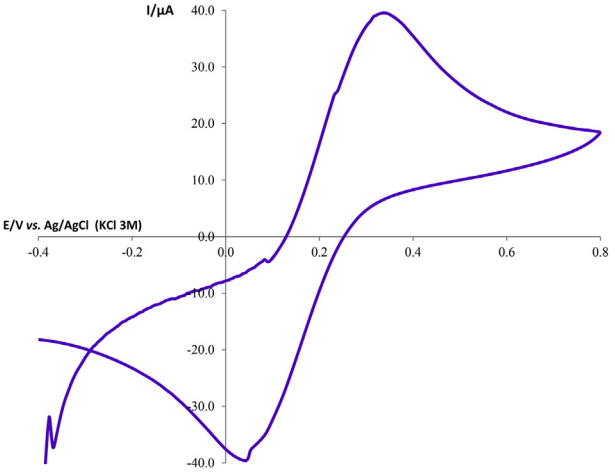

Fig. 10 – Cyclic voltammogram of GCE/GNMO NSs.

Cyclic voltammetry (CV) curve was used for investigation of electrochemical property of the GNMO NSs. In CV experiments, scan rate was 100 mVs^{-1}, supporting electrolyte was a buffer solution of 0.2 M phosphate; and three electrodes including $Ag/AgCl/KCl_{sat}$ (reference electrode), glassy carbon electrode (GCE) modified GCMO NSs (working electrode) and Pt wire (counter electrode) were employed. The CV technique was performed on the surface of the GCE. The CV curve of the GNMO NSs in Fig. 10 shows both cathodic and anodic peak currents. Therefore, the NSs can accelerate the electron transfer at the surface of electrode and act as an appropriate electrocatalyst. The cathodic and anodic peak currents are 39 and −40 μA, respectively.

Conclusions

Using combustion method we have synthesized the GNMO NSs, for the first time to our knowledge. The DRS, VSM and CV results have enabled us to determine the optical, magnetic and electrochemical behaviors of the NSs. We have also for the first time investigated effects of the saccharides and calcination temperature in the synthesis of GNMO NSs, for reaching the optimized condition. The optimum sample was prepared in the presence of the glucose at 1000 °C. This work is the first report of photocatalytic study of the GNMO NSs.

Acknowledgments

Authors are grateful to the council of Iran National Science Foundation (INSF) and University of Kashan for supporting this work by Grant No (159271/8111990).

REFERENCES

[1] Bull CL, Gleeson D, Knight KS. J Phys: Condens Matter 2003;15:4927.
[2] Bull CL, McMillan PF. J Solid State Chem 2004;177:2323.
[3] Sahu B, Raut S, Kaushik SD, Singh AK. AIP Conf. Proc. 2015;1665:140032.
[4] Dankov SY, Tishin AM, Pecharsky VK, Gschneidner KA. Phys Rev B 1998;57:3478.
[5] Pecharsky VK, Gschneidner JKA. Phys Rev Lett 1997;78:4494.
[6] Kakarla DC, Jyothinagaram KM, Das AK, Adyam V, Viehland D. J Am Ceram Soc 2014;97:2858.
[7] Zhao HJ, Liu XQ, Chen XM, Bellaiche L. Phys Rev B 2014;90:195147.
[8] Zhao HJ, Ren W, Yang Y, Iniguez J, Chen XM, Bellaiche L. Nat Commun 2014;5:4021.
[9] Choudhury D, Mandal P, Mathieu R, Hazarika A, Rajan S, Sundaresan A, et al. Phys Rev Lett 2012;108:127201.
[10] Chakraborty T, Nhalil H, Yadav R, Wagh AA, Elizabeth S. J Magn Magn Mater 2017;428:59.
[11] Krishna Murthy J, Chandrasekhar KD, Murugavel S, Venimadhav A. J Mater Chem C 2015;3:836.
[12] Sharma G, Saha J, Kaushik SD, Siruguri V, Patnaik S. Appl Phys Lett 2013;103:012903.
[13] Yáñez-Vilar S, Mun ED, Zapf VS, Ueland BG, Gardner JS, Thompson JD, et al. Phys Rev B 2011;84:134427.
[14] Mohapatra SR, Sahu B, Kaushik SD, Singh AK. AIP Conf. Proc. 2016;1731:130043.
[15] Krishna Murthy J, Venimadhav A. J Phys D: Appl Phys 2014;47:445002.
[16] Balli M, Fournier P, Jandl S, Gospodinov MM. J Appl Phys 2014;115:173904.
[17] Balli M, Fournier P, Jandl S, Truong KD, Gospodinov MM. J Appl Phys 2014;116:073907.
[18] Goodenough JB, Wold A, Arnott RJ, Manjuk N. Phys. Rev. 1961;24:373.
[19] Oh SH, Choi HY, Moon JY, Kim MK, Jo Y, Lee N, et al. J Phys D: Appl Phys 2015;48:445001.
[20] Mohapatra SR, Sahu B, Raut S, Kaushik SD, Singh AK. AIP Conf. Proc. 2015;1665:140032.
[21] M. Honda, T. Goto, T. Owashi, A.G. Rozhin, S. Yamaguchi, T. Ito, S.A. Kulinich, Phys Chem Chem Phys 18 (20160 23628–23637.
[22] Reddy KR, Sin BC, Yoo CH, Park W, Ryu KS, Lee JS, et al. Scripta Mater 2008;58:1010–3.
[23] Reddy NL, Rao VN, Kumari MM, Kakarla RR, Ravi P, Sathish M, et al. Inamuddin, Environ. Chem. Lett. 2018;16:765–96.
[24] Zhang YP, Lee SH, Reddy KR, Gopalan AI, Lee KP. J Appl Polym Sci 2007;104:2743–50.
[25] Reddy KR, Hassan M, Gomes VG. Appl Catal Gen 2015;489:1–16.
[26] Hassan M, Haque E, Reddy KR, Minett AI, Chen J, Gomes VG. Nanoscale 2014;6:11988–94.
[27] Reddy KR, Gomes VG, Hassan M. Mater Res Express 2014;1, 015012.
[28] Cakici M, Kakarla RR, Alonso-Marroquin F. Chem Eng J 2017;309:151–8.
[29] Mahdiani M, Sobhani A, Salavati-Niasari M. Separ Purif Technol 2017;185:140.
[30] Sobhani A, Salavati-Niasari M. J Mater Sci: Mater Electron 2015;26:6831.
[31] Esmaeili-Zare M, Salavati-Niasari M, Sobhani A. J Ind Eng Chem 2014;20:3518.
[32] Jafari M, Sobhani A, Salavati-Niasari M. J Ind Eng Chem 2014;20:3775.
[33] Ansari F, Sobhani A, Salavati-Niasari M. J Colloid Interface Sci 2018;514:723.
[34] Salavati-Niasari M, Sobhani A. High Temp Mater Process 2012;31:157.
[35] Salavati-Niasari M, Sobhani A, khoshrooz S, Mirzanasiri N. J Cluster Sci 2014;25:937.
[36] Albargi H, Alqahtani M, Blythe HJ, Fox AM, Andreev N, Chichkov V, et al. Thin Solid Films 2018;645:326.
[37] Sobhani A, Salavati-Niasari M. Superlattice Microst 2014;65:79.
[38] Booth R, Fillman R, Whitaker H, Nag A, Tiwari R, Ramanujachary K, et al. Mater Res Bull 2009;44:1559.
[39] Kakarla DC, Jyothinagaram KM, Das AK, Adyam V. J Am Ceram Soc 2014;97:2858.
[40] Goodenough JB, Wold A, Arnott RJ, Menyuk N. Phys. Rev. 1961;124:373.
[41] Blasse G. J Phys Chem Solid 1965;26:1969.
[42] Chen X, Liu L, Feng Y, Wang L, Bian Z, Li H, et al. Mater Today 2017;20:501–6.
[43] Raghava Reddy K, Nakata K, Ochiai T, Murakami T, Tryk DA, Fujishima A. J Nanosci Nanotechnol 2011;11:3692–5.
[44] Raghava Reddy K, Karthik KV, Benaka Prasad SB, Soni SK, Jeong HM, Raghu AV. Polyhedron 2016;120:169–74.